Journal of ELECTRONIC MATERIALS, Vol. 45, No. 1, 2016
DOI: 10.1007/s11664-015-4189-3
© 2015 The Minerals, Metals & Materials Society

# Effects of Cooling Rate on the Microstructure and Morphology of Sn-3.0Ag-0.5Cu Solder

HWA-TENG LEE[1,2] and KUO-CHEN HUANG[1,3]

1.—Department of Mechanical Engineering, National Cheng Kung University, No.1, University Road, Tainan 701, Taiwan, ROC. 2.—e-mail: htlee@mail.ncku.edu.tw. 3.—e-mail: a49221137@hotmail.com

This study explored the effect of the cooling rate on the microstructure and morphology of Sn-3.0Ag-0.5Cu (SAC305) lead-free solder. In the experiments, rapid cooling (P1: 63.17°C/s) of SAC305 solder resulted in high tensile strength (60.8 MPa) with no significant loss in ductility (strain >40%) due to the formation of fine-grained primary $\beta$-Sn (average size ~14 $\mu$m) surrounded by a network-like fine eutectic structure consisting of $\beta$-Sn and particle-like $Ag_3Sn$ compound. As the cooling rate was reduced, the morphology of the $Ag_3Sn$ compound evolved progressively from a particle- to a needle-like form and finally to a leaf- or plate-like form. The cooling rate significantly affected the $\beta$-Sn grain size and the morphology of the $Ag_3Sn$ compound. Water cooling (at the fastest cooling rate of 100°C/s) of a solder sample resulted in a microstructure consisting of the finest structure of $Ag_3Sn$ and $\beta$-Sn with no $Cu_6Sn_5$, consequently exhibiting the highest hardness of the various specimens. By contrast, after cooling at the slowest rate of 0.008°C/s, the sample exhibited a coarse eutectic structure consisting of large plate-like $Ag_3Sn$ compound and isolated long rod-like $Cu_6Sn_5$ precipitates. This coarse structure resulted in both lower hardness and poorer tensile strength.

**Key words:** Sn-Ag-Cu, cooling rate, $Ag_3Sn$, $Cu_6Sn_5$

## INTRODUCTION

Solder alloy is used extensively in the electronics packaging industry for soldering electronic modules and boards, realizing heat sinks, and achieving signal connections and electrical transfer. In addition, soldering also enhances the mechanical strength of the package, thus improving its ability to withstand external impact. However, with the continuing trend toward weight reduction and device miniaturization, the reliability of solder joints in high density, thin, three-dimensional (3D) packages has become an important concern.

According to the phase diagram of Sn-Ag-Cu solder,[1] Sn-Ag-Cu near-eutectic solder contains three eutectic compounds, namely $\beta$-Sn, $\varepsilon$-$Ag_3Sn$, and $\eta$-$Cu_6Sn_5$. Previous studies have reported formation of plate-like preliminarily separated $Ag_3Sn$ compound during solidification of Sn-Ag-Cu solder.[2] The coarsening effect of this compound has a profound effect on the mechanical properties and reliability of the solder joint. In general, the formation and growth of eutectic compounds are determined principally by the alloy content, diffusion rate, cooling rate, and solidification time. In the solder reflow process, the cooling rate in the solidification stage is of critical importance, since an improper cooling rate coarsens the phases in the solder matrix, thereby degrading the mechanical properties of the joint. In extreme cases, microcracks may occur in the solder joint, thereby reducing the reliability of the joint and even damaging the printed circuit board (PCB) substrate.[3–5] It has been reported that, as the cooling rate is decreased and the crystallization time increased, the $Ag_3Sn$ compound may exhibit different morphologies, namely spherical, needle-shaped, and plate-like.[5–9] Coarsened $Ag_3Sn$ compound obtained under slower

(Received July 19, 2015; accepted October 27, 2015; published online November 30, 2015)

cooler rates results in a decrease of both hardness and strength, and should thus be avoided in practical soldering applications since this may lead to physical rupturing of the joint.[3,5,10,11]

To enhance the mechanical properties and fatigue durability of SAC solder joints, soldering conditions should be carefully controlled to obtain fine microstructure during the solidification stage. Many studies have shown that different cooling rates result in different microstructural patterns of the solder.[12–14] Kim et al.[3] showed that Sn-Ag solder has excellent mechanical properties due to its fine net-like eutectic structure. However, a lower cooling rate and higher Ag content affect the distribution and size of the $\beta$-Sn dendritic phase and net-like eutectic structure. More specifically, coarsening of the eutectic structure occurs as the cooling rate is reduced, and hence the mechanical properties are correspondingly reduced.

Shen et al.[15] showed that massive $Cu_6Sn_5$ phase is precipitated in Sn-1.0Cu solder at low cooling rate (i.e., 0.09°C/s). However, a fine network-like eutectic $Cu_6Sn_5$ structure is formed uniformly around the primary $\beta$-Sn phase in Sn-0.7Cu solder when cooled at a higher rate of 55.3°C/s. Sigelko[16] mixed Sn-Ag solder with $Cu_6Sn_5$ particles and cooled the specimens at different rates using stainless steel (5.5°C/s) and firebrick (2.33°C/s) as the heat transfer medium, respectively. The results showed that the refinement and dispersive hardening effect of the $Cu_6Sn_5$ particles in the rapidly cooled samples was more pronounced than for the slowly cooled specimens. In addition, the samples cooled at high cooling rate were found to have higher tensile strength. Müller[17] studied the effect of cooling rate on the microstructure of Sn-3.8Ag-0.7Cu, Sn-3.0Ag-0.5Cu, and Sn-3.5Ag-0.4Cu lead-free solders. It was shown that the size of the intermetallic compounds (IMCs) and $\beta$-Sn dendrites decreased as the cooling rate was increased, with the change in size being determined by the degree of undercooling, the solidification duration, and the solder alloying elements. More specifically, under rapid cooling, the degree of undercooling increases and hence the latent heat is carried away more rapidly. As a result, nucleation is accelerated, and thus only limited growth of IMCs occurs. The results also showed that SAC solders with Cu content lower than 0.7 wt.% contain no rod-shaped $Cu_6Sn_5$ phase in the solidified morphology. Ochoa et al.[4,18] and Kang et al.[2] studied the effects of solidification rate on the microstructures of Sn-Ag and Sn-Ag-Cu solders, respectively, and found that plate-like $Ag_3Sn$ compound was formed for high Ag content and slow cooling conditions. Moon et al.[19] reported that the formation of massive $Ag_3Sn$ compound can be attributed to the difference in the degree of undercooling for $Ag_3Sn$ and $\beta$-Sn nucleation, respectively. In general, $\beta$-Sn nucleation requires a greater degree of undercooling than $Ag_3Sn$. Consequently, higher Ag content and slower cooling rate cause the $Ag_3Sn$ phase to solidify and grow gradually to form massive $Ag_3Sn$ as the solidification process proceeds.

The above-cited studies show that the cooling rate during solidification of SAC solders plays an important role in determining the microstructural evolution and morphological changes, and therefore has a significant effect on the mechanical properties of the solder. However, the literature lacks a systematic study of the changes and evolution of the microstructure and IMCs formed in SAC lead-free solder. Accordingly, this study investigated the microstructural changes and morphological evolution of lead-free Sn-3.0Ag-0.5Cu solder subjected to various cooling rates in the range of 0.008°C/s to 100°C/s during the reflow soldering process.

## EXPERIMENTAL PROCEDURES

The continuous cooling rate behavior of SAC solder was investigated using an improved Jominy testing method. Figure 1 presents a schematic illustration of the cooling test. Briefly, a SAC305 solder ingot was placed in a tin furnace and heated to 250°C in accordance with the commonly used reflow soldering temperature for Sn-Ag-Cu solder (i.e., 230°C to 245°C, ≤20 s). The molten solder was then poured into a hollow round tube made of 304 stainless steel. The tube had internal diameter of 15 mm, height of 45 mm, and thickness of 1 mm. The tube was wrapped tightly with cotton thermal insulation to avoid heat dissipation from the inside. Moreover, the base of the tube was placed on a cast aluminum heat sink (80 mm × 50 mm × 20 mm) immersed in water at temperature of 8°C. The temperature distribution within the solder during the cooling process was monitored using K-type AWG30 thermocouples connected to a GL 450 temperature measuring system. The thermocouples were placed at vertical distances of 0 mm, 10 mm, 20 mm, and 30 mm from the heat sink, respectively, being labeled as P1 to P4, respectively. Histories of temperature versus time were traced accordingly. Solidified samples from each of the four measurement points (P1 to P4) were prepared by cold mounting, grinding, polishing, and etching for subsequent metallographic inspection. The morphological changes in the cooled samples were observed using an optical microscope (OM, Leitz Metallux3) and a scanning electron microscope (SEM, FEI Quanta 400F). In addition, the hardness was measured using a Vickers microhardness tester. The hardness was evaluated over five repeated tests for each sample. Tensile test samples with the configuration and dimensions shown in Fig. 2a were prepared using wire electrical discharge machining (WEDM). Due to the limited size of the bulk samples, the dimensions of the test specimens were scaled down proportionally from those prescribed in the ASTM E8 M standard, as shown in Fig. 2b. The tensile tests were performed under room-temperature (25°C) conditions at constant strain rate of $2.98 \times 10^{-3}$ $s^{-1}$ (0.5 mm/min) in every case.

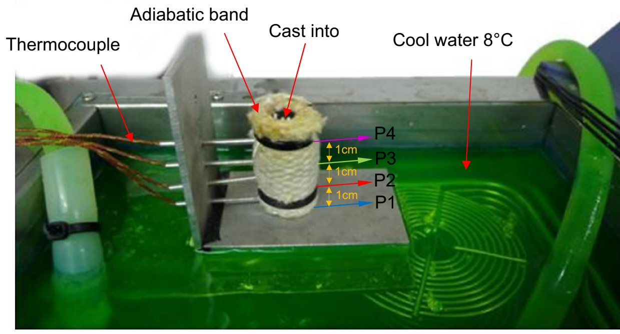


Fig. 1. Schematic diagram of continuous cooling experiment and temperature measurement.

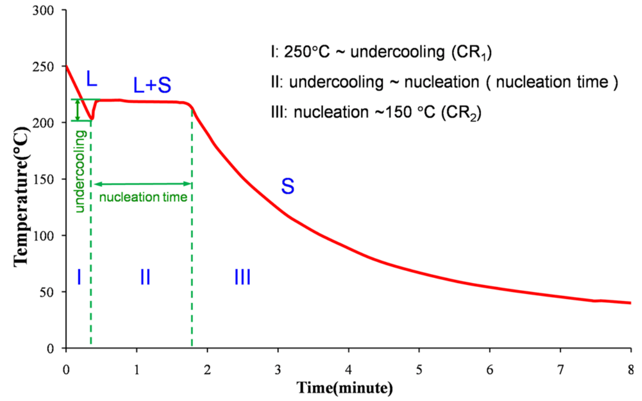


Fig. 3. Analysis of cooling curve (air cooling).

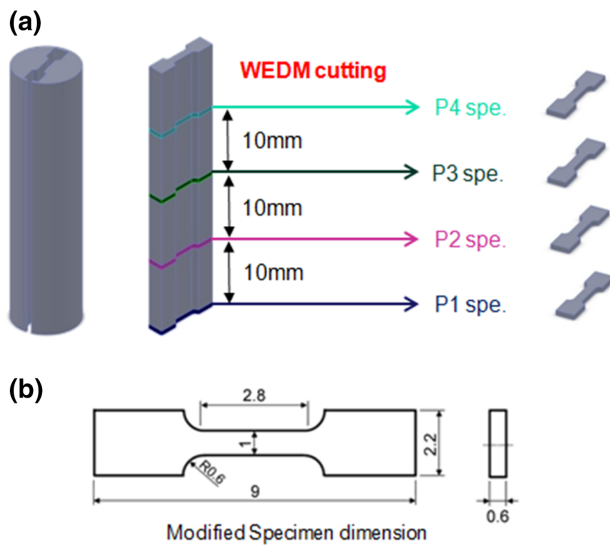


Fig. 2. (a) Tensile specimen production methods (units: mm). (b) Sketch of proportional tensile specimen (units: mm).

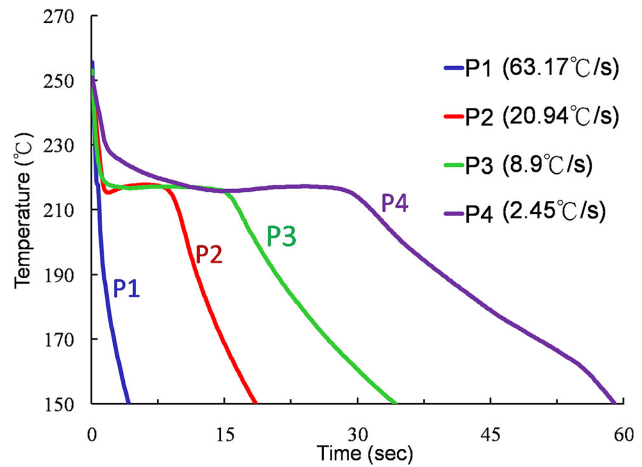


Fig. 4. Cooling curves at various locations (P1 to P4).

## RESULTS AND DISCUSSION

### Continuous Cooling Rate Curves

Figure 3 shows a typical cooling curve for a SAC305 sample cooled in air. As shown, the solidification process comprises three main stages: In stage I (250°C—undercooling), nucleation does not occur immediately as the eutectic temperature is reached. Rather, undercooling occurs and the sample cools instantaneously to a point lower than the eutectic temperature. The latent heat, caused by nucleation, released during the undercooling process causes the temperature to rise again to the eutectic point and to then remain constant as the solidification process proceeds; In stage II (nucleation and solidification), the temperature remains constant during the proceeding process of nucleation and solidification, but decreases again as the remaining liquid phase transforms to solid phase (i.e., the solidification process completes). In stage III, the solidified solder cools continuously to ambient temperature.

**Table I. Primary cooling rate and nucleation time for different points (P1 to P4) in the continuous cooling experiment**

| Material | Method | Position | | | |
|---|---|---|---|---|---|
| | | P1 | P2 | P3 | P4 |
| SAC305 | Cooling rate (°C/s) | 63.17 | 20.94 | 8.9 | 2.45 |
| | Nucleation time (s) | 0.1 | 7.1 | 8.8 | 14.1 |

Figure 4 shows the measured cooling rate and nucleation time at points P1 to P4 of the SAC305 sample cooled in water at 8°C. The total crystallization time for nucleation at points P1 to P4 is 0.1 s, 7.1 s, 8.8 s, and 14.4 s, respectively, as shown in Table I. Following prolonged soaking at a eutectic temperature, the IMCs diffuse and grow into a plate-like morphology, resulting in poor mechanical properties.[13] According to eutectic growth theory,

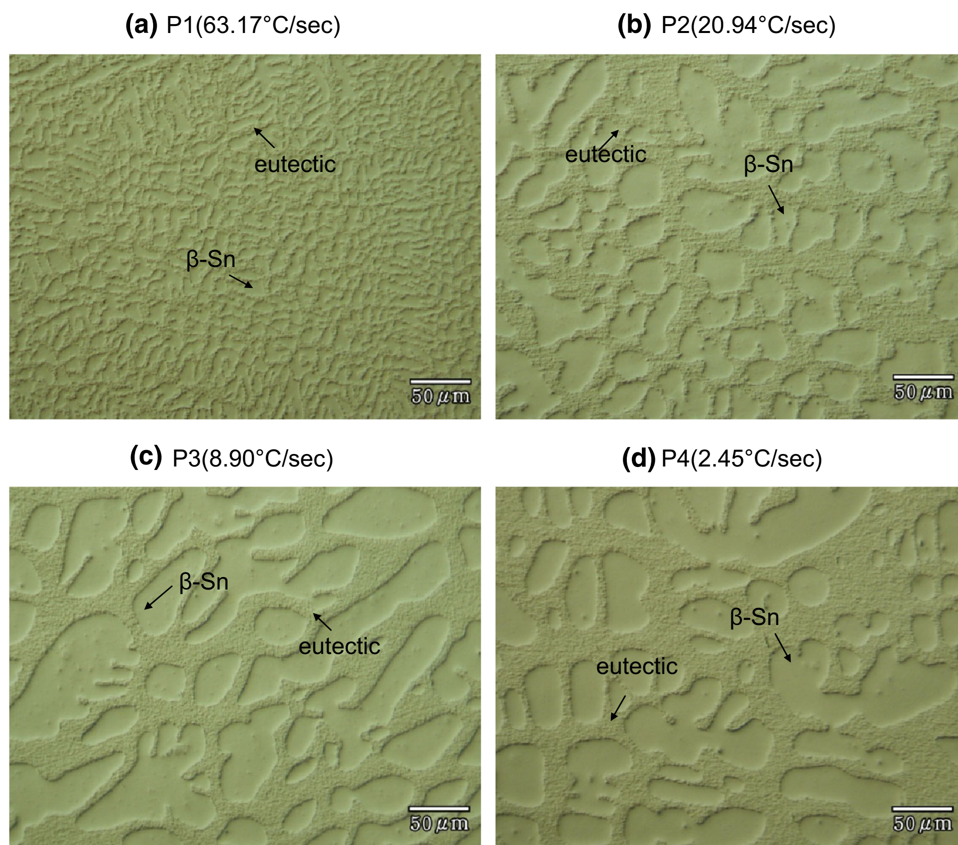


Fig. 5. Microstructure at various locations in the continuous cooling experiment: (a) P1, (b) P2, (c) P3, and (d) P4 (water cooling at 8°C).

high undercooling prompts rapid growth of the eutectic compounds and shorter crystallization time. At point P1 (which experiences a rapid cooling rate due to its close proximity to the heat sink), the undercooling effect is enhanced. However, in the present samples, the suppressed undercooling phenomenon could not be reliably detected, even using the adopted temperature tracing system with sensing speed of 100 ms/point. Thus, the temperature history at point P1 shows only a sharp temperature drop (Fig. 4). By contrast, the temperature history at point P2 exhibits a significant undercooling effect. Points P3 and P4 are located at greater distance from the heat sink and therefore experience more gradual heat transfer. Moreover, the heat loss is also moderated via heat transfer from the upper surface of the sample. Consequently, undercooling is no longer required for solidification at the eutectic temperature, and latent heat dissipation further compensates the heat loss. As a result, a noticeable plateau occurs in the temperature history during the solidification process (Fig. 4).

## Effect of Cooling Rate on Solder Microstructure

The influence of the cooling rate on the microstructure of the SAC305 samples was examined by means of OM and SEM observations. As shown in Fig. 5, the microstructure at point P1 has the finest microstructure among the four samples. Moreover, the cooling rate is equal to 63.17°C/s. As expected, the cooling rate decreases with increasing distance from the heat sink, i.e., 20.94°C/s, 8.9°C/s, and 2.45°C/s at points P2, P3, and P4, respectively. Moreover, an apparent coarsening of the microstructure takes place as the cooling rate is reduced. Figure 5 shows enlarged land-like $\beta$-Sn grains embedded in the eutectic network. Based on inspection of SEM images, the size of $\beta$-Sn grains at points P1 to P4 was estimated to be approximately 30 $\mu m^2$, 380 $\mu m^2$, 550 $\mu m^2$, and 620 $\mu m^2$, respectively. In other words, the density of the eutectic structure decreased remarkably as the cooling rate was decreased. Snugovsky et al.[20] found that, when the Ag and Cu content is lower than the Sn-Ag-Cu eutectic composition, the volume ratio of Sn dendrites increases with increasing cooling rate, while the size of the Sn dendrites decreases. However, higher Ag content causes the volume ratio of Sn dendrites to decrease for higher cooling rates. Since the tests performed in the present study involve nonequilibrium cooling solidification, primary $\beta$-Sn phase forms prior to eutectic formation. Subsequently, networked eutectic structure consisting of phases such as $Cu_6Sn_5$, $Ag_3Sn$, and $\beta$-Sn then forms

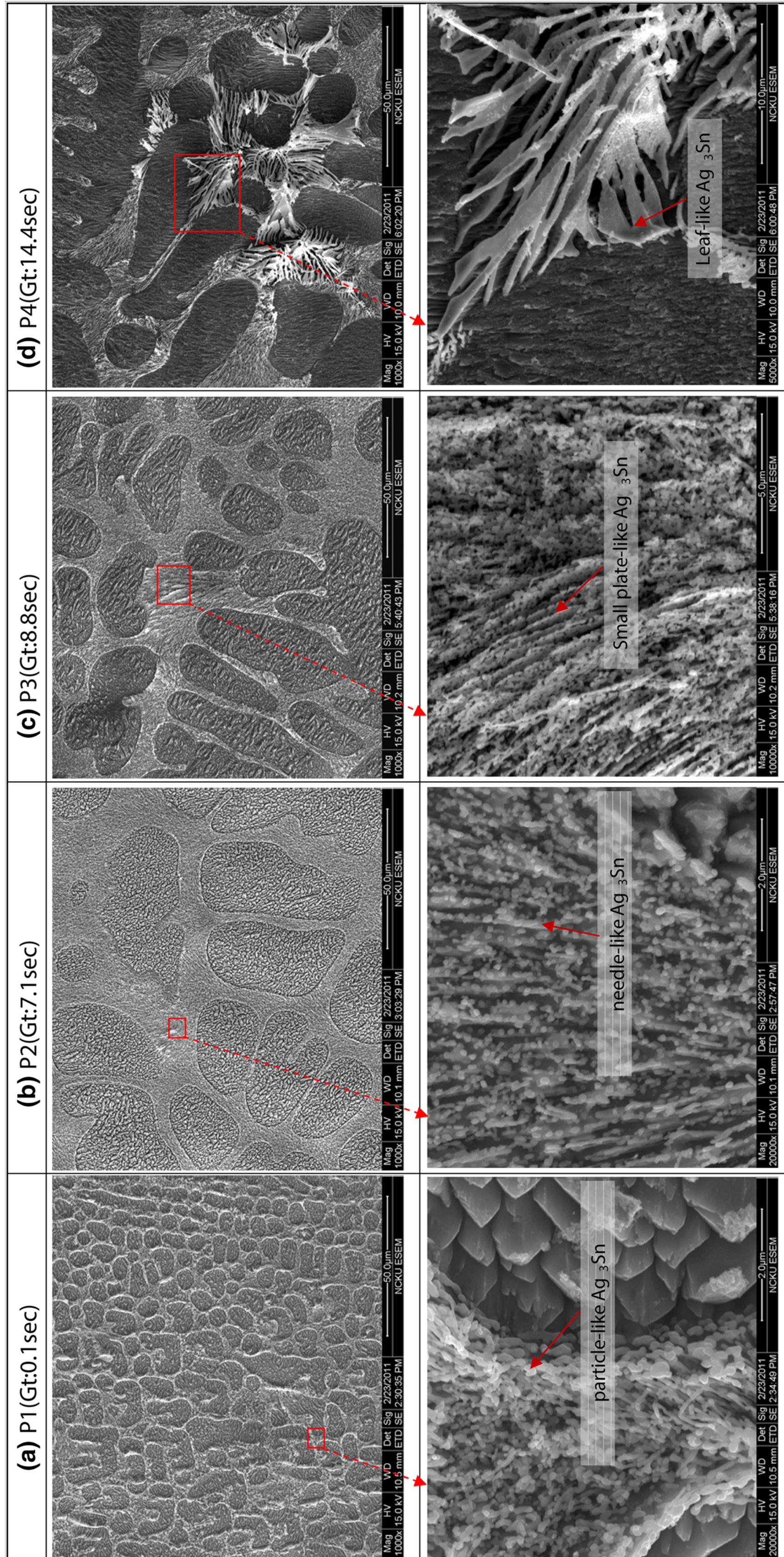


Fig. 6. Three-dimensional (3D) morphology of $Ag_3Sn$ compound at various cooling rates: (a) P1, (b) P2, (c) P3, and (d) P4.

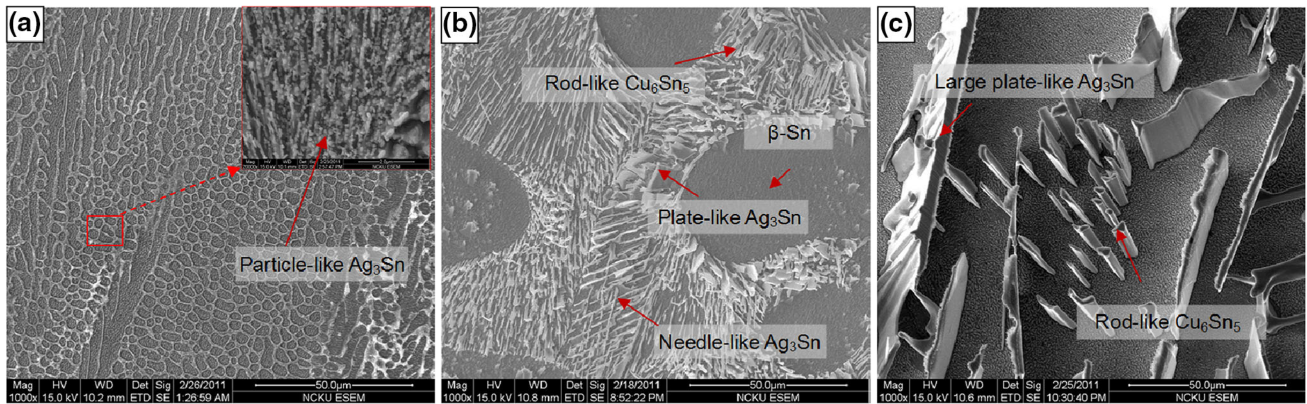


Fig. 7. Microstructure of (a) WC, (b) AC, and (c) FC solder joint samples far from the interfacial layer.

around the original $\beta$-Sn phase as the cooling process proceeds, as shown in Fig. 5. Kim et al.[3] indicated that the volume fraction of eutectic phase in Sn-Ag-Cu solder increases with increasing Ag content. Moreover, the distribution and size of the $\beta$-Sn and eutectic network structure are both influenced by the cooling rate. For a higher cooling rate (i.e., point P1 in the present sample), the primary $\beta$-Sn phase has a fine characteristic with size of approximately 14 $\mu$m (Figs. 5a and 6a). The primary $\beta$-Sn phase is separated by the network-like eutectic phase consisting of $\beta$-Sn and fine-grained $Ag_3Sn$ particles ($\leq$1 $\mu$m, Fig. 6a). The spacing between the primary $\beta$-Sn is relatively small. Consequently, a stressed state is induced in the microstructure, and hence the solder strength is improved. In general, the solder strength is determined by the size and distribution of primary $\beta$-Sn phase and eutectic phase. Observing the microstructures at points P1 to P4, it is found that the amount of $\beta$-Sn phase increased with increasing cooling rate. Using the linear intercept method, the average $\beta$-Sn grain size at points P1 to P4 was found to be approximately 14 $\mu$m, 42 $\mu$m, 61 $\mu$m, and 72 $\mu$m, respectively. Meanwhile, the volume fraction of $\beta$-Sn at the corresponding positions was around 27.8%, 42.5%, 50.2%, and 55.3%, respectively. In other words, as the $\beta$-Sn phase coarsened, the networked eutectic phase also became looser or relaxed due to coarsening of the $Ag_3Sn$ compound within the eutectic phase, as shown in Fig. 6. Further observation of the IMCs revealed that the $Ag_3Sn$ compound had a particle-like characteristic at point P1 with average size $\leq$1 $\mu$m. This result is consistent with the findings of Ochoa[14] that fine spherical $Ag_3Sn$ compound is generated under rapid cooling due to nucleation and the resulting constraint imposed on growth. However, as the cooling rate was decreased, the time available for diffusion and crystal growth increased, and hence the morphology of the $Ag_3Sn$ compound underwent the following transformation: particle-like $\rightarrow$ needle-like $\rightarrow$ plate-like $\rightarrow$ leaf-like (at points P1 to P4, respectively). The high-magnification image presented in Fig. 6c shows that the $Ag_3Sn$ compound in the sample located at point P3 consisted of many irregular flat slices. However, the morphology changed to a leaf- or plate-like form at point P4 under the effects of a lower cooling rate (2.45°C/s). Overall, the results show that the volume fraction of $\beta$-Sn increases with decreasing cooling rate, accompanied by coarsening of the $Ag_3Sn$ compound and a change in its morphological appearance. As discussed below, the microstructural and morphological changes induced under a slower cooling rate lead to a significant reduction in the mechanical properties of the solder.

For comparison, experiments were also performed in which SAC305 samples were cooled in water cooling (WC), air cooling (AC), and a furnace cooling (FC), respectively. The results are shown in Fig. 7. The water-cooled sample, with the maximum cooling rate of 100°C/s, consisted almost exclusively of particle-like $Ag_3Sn$ phase in a eutectic network. Notably, no $Cu_6Sn_5$ phase was observed. By contrast, the sample cooled in air (cooling rate of 2.09°C/s) contained not only plate-like $Ag_3Sn$ compound but also rod-like $Cu_6Sn_5$ phase, as indicated by the arrow and identified by energy dispersive x-ray spectroscopy (EDS) analysis. Finally, the SAC305 sample cooled in the furnace (cooling rate of 0.008°C/s) exhibited a coarsened eutectic structure consisting of large plate-like $Ag_3Sn$ and isolated rod-like $Cu_6Sn_5$ precipitates.

## Effect of Cooling Rate on Microhardness

Figure 8 shows the microhardness of the SAC305 samples cooled under different cooling rates. It is observed that the hardness increased with increasing cooling rate. The sample cooled at the lowest cooling rate of 0.008°C/s had hardness of HV $14.0 \pm 0.62$. However, as the cooling rate was increased, the hardness increased to HV $14.9 \pm 0.39$, HV $15.8 \pm 0.65$, HV $16.5 \pm 0.36$, HV $17.4 \pm 0.48$, HV $19.5 \pm 0.39$, and finally HV

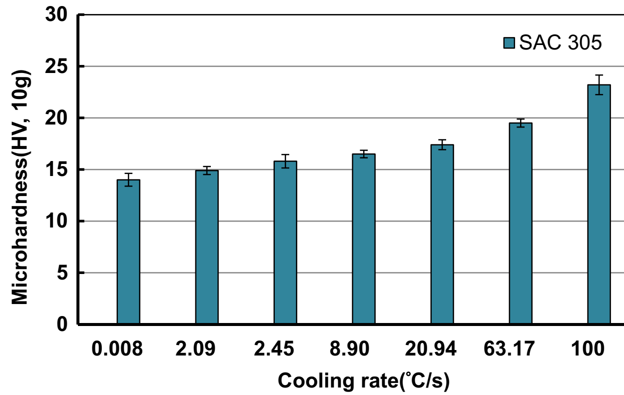


Fig. 8. Effect of different cooling rates on microhardness (units: HV).

$23.2 \pm 0.95$ under the fastest cooling rate of 100.00°C/s. Figure 9 shows the correlation between the evolution of the cooled microstructure and the cooling rate. It is seen that significant coarsening of the $Ag_3Sn$ and $Cu_6Sn_5$ IMCs occurs as the cooling rate is reduced, leading to a notable reduction in the hardness as a result. Deng et al.[21] showed that the microhardness of $Ag_3Sn$ is around 15 times that of pure Sn and 12 times that of the eutectic structure ($\beta$-Sn + $Ag_3Sn$). In other words, the microhardness of $Ag_3Sn$ is far greater than that of $\beta$-Sn. Thus, in the present samples, the finer eutectic structure and smaller $\beta$-Sn phase obtained at higher cooling rate result in greater hardness.

## Effect of Cooling Rate on Tensile Strength of Solder

Figure 10 shows the load–stroke curves for the samples cooled at different cooling rates (i.e., points P1 to P4). It is observed that the tensile strength increased significantly as the cooling rate was increased. The sample cooled at 63.17°C/s exhibited both the highest tensile strength (60.8 MPa) of the various samples and the greatest toughness due to the presence of fine and uniformly distributed $\beta$-Sn particles in the eutectic network and $Ag_3Sn$ compound with fine, particle-like morphology. As the cooling rate was reduced, the $Ag_3Sn$ compound transformed initially to a needle-like form, then to a leaf- or plate-like form. Moreover, the eutectic network changed from a fine network-like phase morphology to a coarsened structure consisting of large plate-like $Ag_3Sn$ compound and isolated rod-like $Cu_6Sn_5$ phase. The changes in the microstructure and morphology caused the tensile strength of the solder to reduce from 60.8 MPa at point P1 to 50.8 MPa, 46.6 MPa, and 39.5 MPa at points P2, P3, and P4, respectively.

Macroscopic observations of tensile-fractured samples revealed that all four specimens (P1 to P4) underwent apparent plastic deformation with necking characteristic at the fracture site. In other words, all four specimens behaved in a ductile

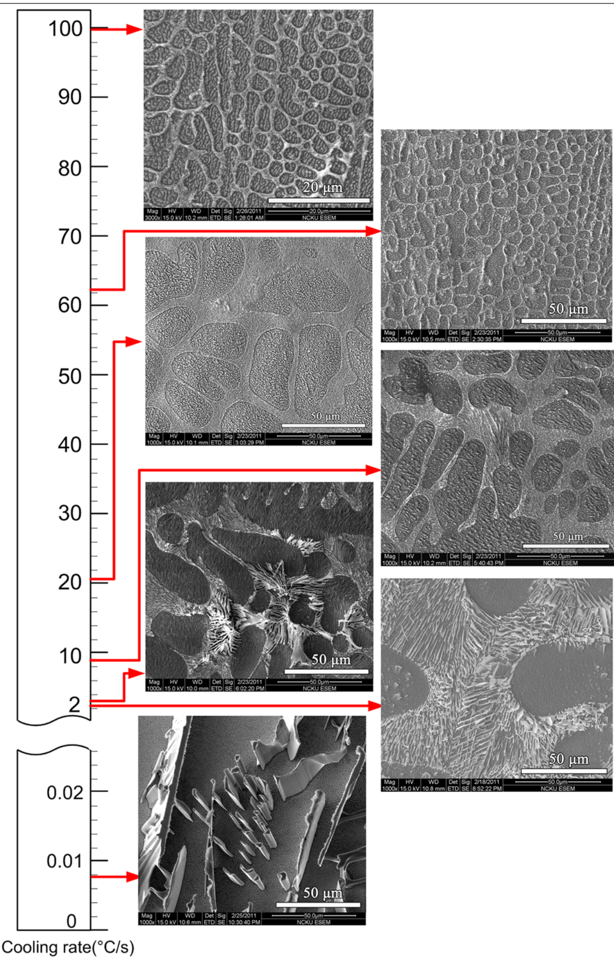


Fig. 9. Continuous cooling rate morphology evolution of SAC305 solder.

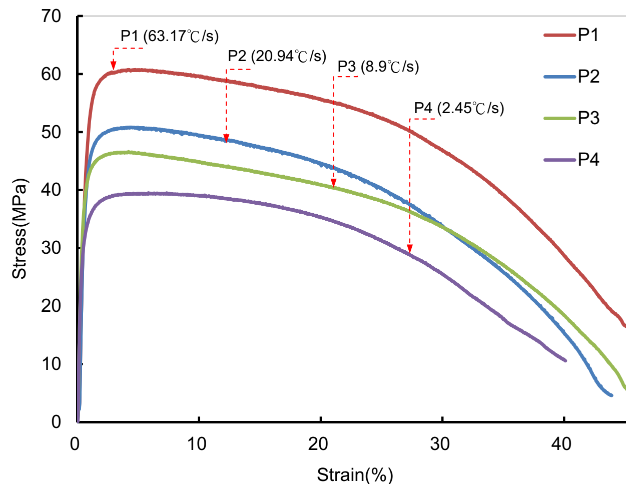


Fig. 10. Stress–strain curves for solder alloy solidified at various cooling rates.

manner under tension. The tensile curves presented in Fig. 10 for the different cooling rates show that the ductility exceeded 40% in each case. Of the

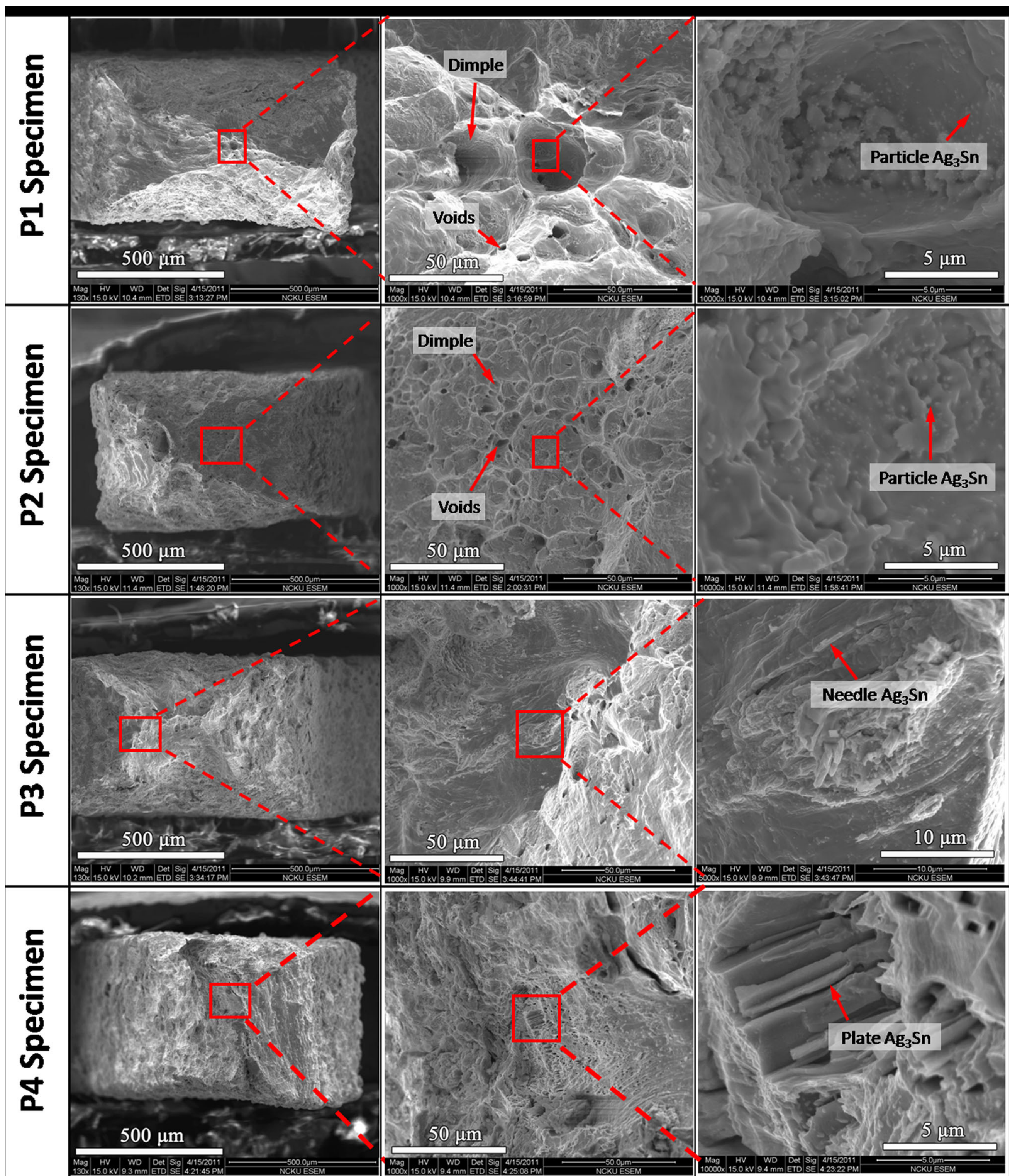


Fig. 11. Tensile fracture surface microstructure of samples P1 to P4.

various samples, that located at point P1 showed not only the highest tensile strength (60.8 MPa) but also the greatest ductility. As discussed above, under rapid cooling, the SAC solder material has a fine and uniformly dispersed microstructure of $\beta$-Sn phase surrounded by a network of eutectic phase consisting of fine dispersed $Ag_3Sn$ particles. The results presented in Fig. 10 show that the stressed state of the fine-grained microstructure, together with the abundance of grain boundaries, prompted a

significant material strengthening effect with no loss in ductility. By contrast, the sample obtained at point P4, characterized by a slower cooling rate, showed the lowest tensile strength (39.5 MPa) and slightly reduced ductility. In general, therefore, the results show that a faster cooling rate is beneficial for improving the strength without loss of toughness of the SAC solder material.

Figure 11 shows the SEM morphologies of the tensile fractured surfaces of the samples obtained at points P1 to P4. The fracture surfaces of the samples from P1 and P2 contained particle-like $Ag_3Sn$ compound, while those of the samples at P3 and P4 contained needle-like $Ag_3Sn$ and plate-like $Ag_3Sn$, respectively. In addition, the samples that experienced a slower cooling rate (P3 and P4) contained fewer cavities and fine slip lines, while those that underwent more rapid cooling (P1 and P2) contained a greater number of cavities and dimples. The greater number of cavities formed at higher cooler rate may be the result of more ready formation and fracture of trapped gas pockets at sites of inclusions or particles within the solder material. By contrast, under slower cooling conditions, the gas within the molten solder material has a greater opportunity to escape from the solidifying microstructure, hence the number of cavities is reduced.

## CONCLUSIONS

The effect of the cooling rate on the solidified microstructure of SAC305 solder was investigated. The experimental results support the following major conclusions:

1. The microstructure and mechanical properties of SAC305 solder are greatly influenced by the cooling rate. More specifically, the tensile strength and hardness both increase with increasing cooling rate due to formation of fine-grained primary $\beta$-Sn phase surrounded by a network-like fine eutectic structure.
2. The solder with rapid cooling (P1: 63.17°C/s) showed high tensile strength (60.8 MPa) among the various samples with no loss in ductility (strain $>40\%$). SEM observations showed that the fracture surface contained a large number of dimples. By contrast, the sample processed with slow cooling (P4: 2.45°C/s) had lower tensile strength of 39.5 MPa and a fracture surface characterized by fewer dimples and greater slip deformation.
3. As the cooling rate was reduced, the morphology of the $Ag_3Sn$ compound formed during the solidification process changed initially from a fine particle-like form to a needle-like form, and finally to a leaf- or plate-like form. Under cooling at continuously reducing cooling rates, $Ag_3Sn$ compound with multiple morphologies generally coexisted within the solidified structure.
4. The solder sample that underwent the maximum cooling rate (water cooling at 100°C/s) showed the finest structure of $Ag_3Sn$ and $\beta$-Sn with no $Cu_6Sn_5$. Consequently, this sample had the highest hardness. By contrast, after the lowest cooling rate (furnace cooling at 0.008°C/s), the microstructure consisted of a coarsened eutectic structure with large plate-like $Ag_3Sn$ compound and isolated long rod-like $Cu_6Sn_5$ precipitates. The mechanical properties were thus correspondingly reduced.

## ACKNOWLEDGEMENTS

The authors gratefully acknowledge financial support of this research by the Ministry of Science and Technology, Republic of China, Taiwan under Grant No. MOST 102-2221-E-006-294-MY3.

## REFERENCES

1. K. Suganuma, *Environmentally Conscious Design and Inverse Manufacturing, 1999 Proceedings EcoDesign'99 (IEEE Xplore)*, (1999), p. 620.
2. S.K. Kang, D.Y. Shih, D. Leonard, D.W. Henderson, T. Gosselin, S.I. Cho, J. Yu, and W.K. Choi, *JOM* 56, 34 (2004).
3. K.S. Kim, S.H. Huh, and K. Suganuma, *Mater. Sci. Eng. A* 333, 106 (2002).
4. F. Ochoa, J.J. Williams, and N. Chawla, *JOM* 55, 56 (2003).
5. L.R. Garcia, W.R. Osório, and A. Garcia, *Mater. Des.* 32, 3008 (2011).
6. J.H.L. Pang, L. Xu, X.Q. Shi, W. Zhou, and S.L. Ngoh, *J. Electron. Mater.* 33, 1219 (2004).
7. H.T. Ma, L. Qu, M.L. Huang, L.Y. Gu, N. Zhao, and L. Wang, *J. Alloys Compd.* 537, 286 (2012).
8. W.R. Osório, L.R. Garcia, L.C. Peixoto, and A. Garcia, *Mater. Des.* 32, 4763 (2011).
9. X. Liu, M. Huang, Y. Zhao, C.M.L. Wu, and L. Wang, *J. Alloys Compd.* 492, 433 (2010).
10. J. Gong, C. Liu, P.P. Conway, and V.V. Silberschmidt, *Mater. Sci. Eng. A* 427, 60 (2006).
11. A.K. Gain, T. Fouzder, Y.C. Chan, A. Sharif, and W.K.C. Yung, *J. Alloys Compd.* 489, 678 (2010).
12. W.R. Osório, J.E. Spinelli, C.R.M. Afonso, L.C. Peixoto, and A. Garcia, *Electrochim. Acta* 56, 8891 (2011).
13. H.T. Lee and Y.F. Chen, *J. Alloys Compd.* 509, 2510 (2011).
14. F. Ochoa, J.J. Williams, and N. Chawla, *J. Electron. Mater.* 32, 1414 (2003).
15. J. Shen, Y.C. Liu, and H.X. Gao, *J. Mater. Sci.* 42, 5375 (2007).
16. J. Sigelko, S. Choi, K.N. Subramanian, J.P. Lucas, and T.R. Bieler, *J. Electron. Mater.* 28, 1184 (1999).
17. M. Muller, S. Wiese, and K.J. Wolter, *Electronics System-integration Technology Conference Dresden* (Germany: IEEE Xplore, 2006), p. 1303.
18. K.S. Kim, S.H. Huh, and K. Suganuma, *J. Alloys Compd.* 352, 226 (2003).
19. K.W. Moon, W.J. Boettinger, U.R. Kattner, F.S. Biancaniello, and C.A. Handwerker, *J. Electron. Mater.* 29, 1122 (2000).
20. L. Snugovsky, P. Snugovsky, D.D. Perovic, and J.W. Rutter, *Mater. Sci. Technol.* 21, 61 (2005).
21. X. Deng, N. Chawla, K.K. Chawla, and M. Koopman, *Acta Mater.* 52, 4291 (2004).